Chiang Mai J. Sci. 2018; 45(2) : 1073-1086
http://epg.science.cmu.ac.th/ejournal/
Contributed Paper

Topoisomerase I Inhibitory Activity and 3D QSAR Studies of Chromone Derivatives

Chirattikan Maicheen [a], Narumol Phosrithong [b], Jiraphun Jittikoon [c] and Jiraporn Ungwitayatorn* [c]

[a] Faculty of Pharmacy, Huachiew Chalermprakiet University, 18/18 Bang Na-Trad Road, Samut Prakarn 10540, Thailand.

[b] Faculty of Pharmacy, Siam University, 38 Petkasem Road, Bangkok 10160, Thailand.

[c] Center of Excellence for Innovation in Drug Design and Discovery, Faculty of Pharmacy, Mahidol University, 447 Sri-Ayudhya Road, Bangkok 10400, Thailand.

* Author for correspondence; e-mail: jiraporn.ung@mahidol.ac.th

Received: 8 December 2016
Accepted: 31 January 2017

ABSTRACT

Topoisomerase I (Top I) is the molecular target for a diverse set of anticancer agents. This study was a continuation of previous work examining the Top I inhibitory activity of a series of chromone derivatives. Nine chromones were evaluated using eukaryotic DNA TOP I drug screening kit. The most potent inhibitor, chromone **20** showed greater inhibitory activity (IC_{50} = 0.83 μM) than the previously reported chromone compounds as well as the known Top I inhibitor, camptothecin. To develop the structure-Top I inhibitory activity relationship, the 3 dimensional quantitative structure-activity relationship (3D QSAR) were performed using comparative molecular field analysis (CoMFA) and comparative molecular similarity indices analysis (CoMSIA). The best CoMFA model gave cross-validated r^2 (q^2) = 0.578 and non cross-validated r^2 = 0.995 while CoMSIA gave q^2 = 0.632, r^2 = 0.996. The contour maps provide the fruitful structural features which are useful for designing new compounds with higher activity.

Keywords: chromone derivatives, topoisomerase I inhibitory activity, CoMFA, CoMSIA

1. INTRODUCTION

DNA topoisomerases are important targets of approved and experimental anticancer drugs. They are essential for a number of cellular processes those involve DNA unwinding including DNA replication, transcription, recombination, and chromatin remodeling [1]. Their functions have been reported to relieve the torsional stress in the DNA helix that is generated as a result of replication, transcription, and other nuclear processes [2-3]. Topoisomerases affect the supercoiling of closed circular DNA and long strands of double-stranded DNA by introducing transient breaks in the phosphodiester backbone and form a covalent phosphotyrosine intermediate with the DNA [4-6]. Based on the mechanism of cleaving DNA, topoisomerases are classified

as type I and type II. Topoisomerase I (Top I), a monomeric enzyme, relaxes superhelical DNA by cleaving one strand of duplex DNA through transesterification of Tyr723 and forms a 3′-phosphotyrosine linkage to the DNA, followed by the unwinding of supercoiled DNA [7-8]. Topoisomerase II (Top II) is dimeric, transiently breaks both strands of duplex DNA, and passes an intact DNA duplex through this transient double-stranded break in an ATP-dependent manner. Without topoisomerases, the DNA cannot replicate normally, therefore the inhibitors of DNA topoisomerases have been used as anticancer agents to stop the proliferation of malignant cells [9-11]. Top II inhibitors include a number of compounds, e.g., etoposide, teniposide and amsacrine, all of which stabilize the covalent binary complex formed between Top II and DNA [9]. There are fewer known inhibitors of Top I, but camptothecin (CPT), an alkaloid extracted from *Camptotheca acuminata* initially discovered because of its potent and broad spectrum antitumor activity [12] has been shown to target at Top I [13]. CPT binds to the Top I-DNA covalent complex, resulting in a ternary complex, and thereby stabilizing it [14-16]. This prevents DNA relegation, therefore causes DNA damage and leading to apoptosis.

Plant-derived flavonoids, low molecular weight polyphenolic compounds, have been reported to inhibit DNA Top I [17-20]. Quercetin and related natural flavone derivatives, such as acacetin, apigenin, kaempferol, and morin, stabilize the covalent DNA topoisomerase I-DNA post-cleavage complex by inhibiting the relegation process [18]. In contrast to CPT, these compounds do not act directly on the catalytic intermediate and also do not interfere with DNA cleavage. Luteolin inhibits the catalytic activity of eukaryotic DNA Top I with an IC_{50} of 5 μM [17]. Luteolin is similar to CPT, with respect to its ability to form the Top I-mediated cleavable complex. But, unlike CPT, luteolin interacts with both free enzyme and substrate DNA. Thus, flavonoids have the potential to be an ideal model for structural requirements of Top I inhibitor and may serve for the development of new anticancer agents.

In our previous study, a series of 25 chromone derivatives (structures as shown in Table 1) have been synthesized and 16 compounds (chromones 1-16, Table 1) have been tested for their inhibitory activity against Top I. Most compounds showed moderate to good Top I inhibitory activity [21]. Chromone **15** (or chromone **11b** as named in the previously study) was found to be the most potent inhibitor with IC_{50} = 1.46 μM whereas CPT possessed IC_{50} = 18.85 μM [22-24]. To continue the study, more 9 chromone derivatives (chromones 17-25) have been evaluated for their Top I inhibitory activity using eukaryotic Top I drug screening kit (TopoGen, Inc., USA). To explore the relationships between the structures of these compounds and their Top I inhibitory activity, a three-dimensional quantitative structure-activity relationship (3D QSAR) study using comparative molecular field analysis (CoMFA) [25] and comparative molecular similarity indices analysis (CoMSIA) [26-27] were also performed in this study.

Table 1. Structures of 25 synthesized chromone derivatives.

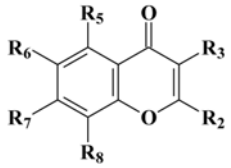

Compd	R_2	R_3	R_5	R_6	R_7	R_8
1	Phenyl	Benzoyl	H	H	O-Benzyl	H
2	Phenyl	Benzoyl	H	H	O-[3′ ″-(OCH_3)-benzoyl]	H
3	Phenyl	Benzoyl	H	H	O-[4′ ″-(OCH_3)-benzoyl]	H
4	Phenyl	Benzoyl	H	H	O-[3′ ″-(NO_2)-benzoyl]	H
5	Phenyl	Benzoyl	H	H	O-[4′ ″-(NO_2)-benzoyl]	H
6	3′-(OCH_3)-phenyl	3″-(OCH_3)-benzoyl	H	H	O-Benzyl	H
7	3′-(OCH_3)-phenyl	3″-(OCH_3)-benzoyl	H	H	O-[3′ ″-(OCH_3)-benzyl]	H
8	3′-(OCH_3)-phenyl	3″-(OCH_3) benzoyl	H	H	O-Benzoyl	H
9	3′-(OCH_3)-phenyl	3″-(OCH_3)-benzoyl	H	H	O-[3′ ″-(OCH_3)-benzoyl]	H
10	3′-(OCH_3)-phenyl	3″-(OCH_3)-benzoyl	H	H	O-[4′ ″-(OCH_3)-benzoyl]	H
11	4′-(OCH_3)-phenyl	4″-(OCH_3)-benzoyl	H	H	O-[3′ ″-(OCH_3)-benzyl]	H
12	4′-(OCH_3)-phenyl	4″-(OCH_3)-benzoyl	H	H	O-Benzoyl	H
13	4′-(OCH_3)-phenyl	4″-(OCH_3)-benzoyl	H	H	O-[3′ ″-(OCH_3)-benzoyl]	H
14	4′-(OCH_3)-phenyl	4″-(OCH_3)-benzoyl	H	H	O-[4′ ″-(OCH_3)-benzoyl]	H
15	4′-(NO_2)-phenyl	4″-(NO_2)-benzoyl	H	H	O-Benzoyl	H
16	4′-(NO_2)-phenyl	4″-(NO_2)-benzoyl	H	H	O-[3′ ″-(NO_2)-benzoyl]	H
17	Phenyl	Benzoyl	H	H	OH	H
18	3′-(OCH_3)-phenyl	3″-(OCH_3)-benzoyl	H	H	OH	H
19	4′-(OCH_3)-phenyl	4″-(OCH_3)-benzoyl	H	H	OH	H
20	4′-(NO_2)-phenyl	4″-(NO_2)-benzoyl	H	H	OH	H
21	4′-(F)-phenyl	4″-(F)-benzoyl	H	H	OH	H
22	4′-(*t*-butyl)-phenyl	4″-(*t*-butyl)-benzoyl	H	H	OH	H
23	3′-(Cl)-phenyl	3″-(Cl)-benzoyl	H	H	OH	H
24	4′-(NO_2)-phenyl	4″-(NO_2)-benzoyl	OH	H	OH	H
25	4′-(NO_2)-phenyl	4″-(NO_2)-benzoyl	H	H	OH	OH

2. MATERIALS AND METHODS

2.1 Chemical Synthesis

All studied chromones were prepared by one pot cyclization reaction modified from the method of Riva *et al.* [28] using phenolic ketone and acid chloride. After the phenolic ester and subsequent β-diketone intermediates were formed, esterification of the free hydroxyl group followed by rearrangement of the acyl group to the β-diketone intermediate, cyclization and dehydration processes, the 2, 3-disubstitued chromone ester was obtained. Hydrolysis of the chromone esters yielded the required chromone derivatives. The chemical structures of the synthesized chromones were elucidated by Fourier transform infrared (FTIR) and proton nuclear magnetic resonances (^{1}H NMR) spectra. Molecular weights of the compounds were determined by high resolution mass spectrometer. More details of the synthesis procedures and spectroscopic

data were reported in reference 29.

2.2 Topoisomerase I Inhibitory Activity Assay

The ability of synthesized chromone compounds to stabilize the formation of the Top I-DNA covalent binary complex was determined using eukaryotic Top I drug screening kit (TopoGen, Inc., USA) (www.topogen.com). Purified Top I was purchased from TopoGen, Inc., USA. Supercoiled DNA (125 ng) was incubated in the presence of Top I (2.5 units), Top I assay buffer (1.5 µL) and synthesized compounds at 37 °C. The concentrations used for the test chromones were 0.1, 1, 10, 20, 40, and 100 µM for chromones **19** and **20**, the rest of the compounds were tested at 100 µM. After 30 minutes, the reactions were terminated by adding 10 % sodium dodecyl sulfate (0.1 volume), and digested with 0.5 mg/mL proteinase K at 37 °C for 30 minutes. Gel loading buffer (1/10 volume) was added into the reaction mixture. Then DNA was separated by loading on 1 % agarose gel. Relaxed DNA was included in the electrophoresis run as markers for DNA topology. CPT (100 µM) was used as positive control. Electrophoresis was conducted at 100 V for 1.5 hours in TAE buffer (Tris-acetate, EDTA, pH 8.0). After electrophoresis, the gels were stained with 0.5 µg/mL ethidium bromide, and photographed under UV light. The amount of nicked DNA was calculated using ImageQuant TL (Image analysis software version 2003). All determinations were performed in triplicate. The percentage of Top I inhibition was calculated using the following equation:

$$\% \text{ Inhibition} = (\text{Amount of nicked DNA}_{sample} \times 100) / \text{Amount of nicked DNA}_{control}$$

where amount of nicked DNA_{sample} was calculated from the band produced by synthesized compound and amount of nicked $DNA_{control}$ was calculated from the band produced by 100 µM CPT.

The IC_{50} values (the concentration of tested compound required to stabilize 50 % of nicked DNA) were determined by interpolation from the calibration curve plotted between % inhibition (relative to the intensity of the band produced by 100 µM CPT) and sample concentrations in log scale. IC_{50} of chromones **19** and **20** were determined.

2.3 3D QSAR Study

The inhibitory activity was converted to log % inhibition and used as dependent variables for 3D QSAR study.

The 3D structures of all studied compounds were modeled with SYBYL-X 2.0 molecular modeling program (Tripos Associates, Saint Louis, MO) using sketch approach. Each structure was first energy minimized using the standard Tripos force field with a distance-dependent dielectric function and the Powell conjugate gradient algorithm. Convergence criteria of 0.01 kcal/(mole.Å) was used for energy minimization. The partial atomic charges were calculated using the Gasteiger-Hückel method. The minimized structures were further optimized by semi-empirical AM1 using MOPAC. The fully geometrical optimized structures were used in the following 3D QSAR study.

2.3.1 Structural alignment

The AM1 optimized molecules were aligned using two criteria, i.e., field fit and align database functions in SYBYL-X 2.0 program. The most active compound, chromone **20**, was used as a template molecule.

In align database command, chromone nucleus was used as substructure to evaluate the best fit. Substructural overlap assumed that the molecules shared a common core of atoms which were overlapped in each molecule of the database. The field fit alignment of molecules was based on trying to increase field similarity within a series of studied molecules. The root-mean-square differences in the sum of steric and electrostatic interaction energies averaged across all (possibly weighted) lattice points, between that molecule and the template was minimized to find the best fit.

2.3.2 CoMFA and CoMSIA setup

CoMFA and CoMSIA were performed using the QSAR option in SYBYL-X 2.0. In CoMFA, the cubic grid space was generated around molecules in the training set based on the molecular volume of the structures. A sp^3-carbon atom was probed with a +1.0 unit charge, 2.0 Å grid spacing, and the default 30 kcal/mole energy cutoff for steric and electrostatic fields.

CoMSIA was performed using steric, electrostatic, hydrophobic, hydrogen bond donor and hydrogen bond acceptor fields. These parameters were evaluated using common probe atom with 1 Å radius, charge +1.0, hydrophobicity +1.0, hydrogen bond donor and acceptor properties +1.0. Similarity indices were calculated using Gaussian-type distance dependence between the probe and the atoms of the molecules of the data set. The value of the attenuation factor a was set to 0.3.

2.3.3 Statistical analysis

Partial least-squares (PLS) methodology was used for all 3D QSAR analyses. The grid had a resolution of 2.0 Å and extended beyond the molecular dimensions by 4.0 Å in all directions. Column filtering was set to 2.0 kcal/mole. CoMFA and CoMSIA models were developed using the conventional stepwise procedure. The optimum number of components used to derive the non-validated model was defined as the number of components leading to the highest cross-validated r^2 (q^2) and the lowest standard error of prediction (SEP). The q^2 values were derived after "leave-one-out" cross-validation. The non-cross-validated models were assessed by the explained variance r^2, standard error of estimate (S) and F ratio. The non cross-validated analyses were used to make prediction of the % inhibition of the chromone compounds from the test set and to display the coefficient contour maps. The actual versus predicted % inhibitions of the test chromone compounds were fitted by linear regression, and the "predictive" r^2, S, and F ratio were determined.

2.3.4 QSAR coefficient contour maps

The visualization of the results of the best CoMFA and CoMSIA models have been performed using the "StDev*Coeff" mapping option contoured by contribution. Favored and disfavored levels fixed at 80% and 20%, respectively. The contours of the CoMFA and CoMSIA steric maps are shown in green (more bulk is favored) and yellow (less bulk is favored). The electrostatic fields of both CoMFA and CoMSIA contours are colored blue (positive charge is favored) and red (negative charge is favored). The contours of the CoMSIA hydrophobic fields are colored yellow (hydrophobic groups enhance activity) and white (hydrophilic groups enhance activity). The hydrogen bond field contours show regions where hydrogen bond acceptors (magenta) on the receptor enhance the activity and hydrogen bond donors (cyan) increase the activity.

2.4 Docking Study

The crystal structure of Top I complexed with CPT (pdb code 1T8I) used in this study was obtained from the Brookhaven Protein Database (http://www.rcsb.org/pdb). Docking was performed by AutoDock program version 4.2 (Scripps Research Institute, USA) using an empirical free energy function and Larmarckian Genetic Algorithm, with an initial population of 150 randomly placed individuals, a maximum number of 106 energy evaluations, a mutation rate of 0.02, and a crossover rate of 0.80. One hundred independent docking runs were performed for each ligand. Results differing by <2.0 Å in positional root-mean-square deviation (RMSD) were clustered together and represented by the result with the most favorable free energy of binding.

3. RESULTS AND DISCUSSION

Topoisomerase I inhibitory activity

In this study, 9 compounds (chromones **17**-**25,** structures as shown in Table 1) were evaluated for their Top I inhibitory activity using eukaryotic Top I drug screening kit which is a specific assay for Top I. Detection of the transient DNA nicks requires trapping the enzyme on DNA in a nicked intermediate complex using protein denaturants, e.g., sodium dodecyl sulfate. The resulting covalent Top I-DNA complexes contain nicked open circular DNA which can be detected by agarose gel electrophoresis (with ethidium bromide). Normally, the process to trap the nicked intermediates is relatively difficult because the half-life of this cleavage complex is rather short. However, CPT can stabilize the intermediate and increases in the nicked DNA product. Thus detection of agents that affect Top I by stabilizing the cleaved intermediate complex can be performed.

The chromone compounds were evaluated for percentage inhibition of Top I at a concentration of 100 μM and results are shown in Table 2. The two most potent compounds, chromones **19** and **20** with 86.89 and 59.67 % inhibition, respectively, were subjected to further determination of IC_{50}. Chromone **20** was found to be more potent (IC_{50} = 0.83 μM) than the previously reported chromone **15** (IC_{50} = 1.46 μM). Chromone **20** also showed higher potency than the structurally related flavonoids, myricetin (IC_{50} = 11.9 μg/mL, 37.39 μM), quercetin (IC_{50} = 12.8 μg/mL, 42.35 μM) and fisetin (IC_{50} = 20.6 μg/mL, 71.97 μM) [17]. Moreover, chromone **20** even exhibited higher potency than irinotecan, the clinically approved CPT analogue, which possessed Top I inhibitory activity for LoVo cells and HT-29 cells with IC_{50} of 15.8 μM and 5.17 μM, respectively [30].

Figure 1 shows results from the ethidium-stained agarose gel. Typically, supercoiled DNA appeared to migrate more rapidly than the nicked DNA due to its supercoiled nature, the DNA fragments became smaller in size and hence experienced less frictional resistance from the gel. This resulted in the migration of supercoiled conformation to be faster than other conformations of DNA. In the presence of chromone compounds, Top I-DNA cleavage complexes, assayed as nicked DNA were observed. Lanes 1-2 in Figures 1a and 1b represented the supercoiled DNA and Top I treated with chromones 20, 17, 19 and 18, respectively. Lanes 5-7 in Figure 1c and lanes 5-6 in Figure 1d were DNA and Top I treated with chromones 23, 22, 21, 25 and 24, respectively. Although the band intensity of the chromone compounds appeared to be weaker than the band caused by CPT, the results indicated the ability of the tested chromones to stabilizing Top I-DNA cleavage complex.

Table 2. Top I inhibitory activity of 9 chromone derivatives.

Compd	% Inhibition		IC_{50} (μM)
	20 μM	100 μM	
17	nd	55.07	nd
18	nd	27.93	nd
19	42.06	86.89	15.24
20	92.00	59.67	0.83
21	nd	44.69	nd
22	nd	47.43	nd
23	nd	49.09	nd
24	nd	36.47	nd
25	nd	35.63	nd

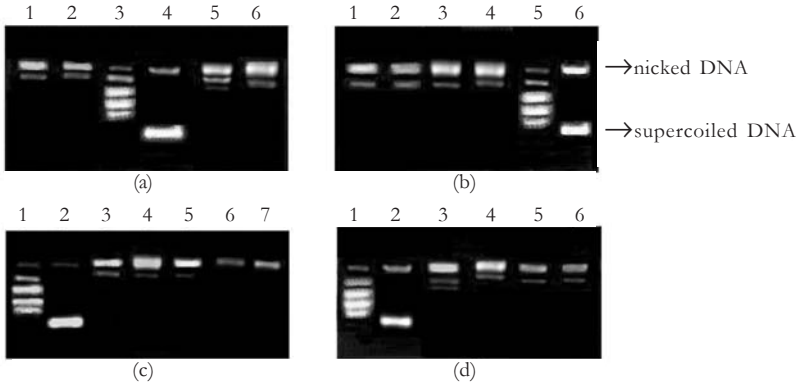

Figure 1. Stabilization of recombinant Top I-DNA complex by chromone compounds, measured after agarose gel electrophoresis. (a) Lanes 1-2 = supercoiled DNA + Top I + chromones **20** and **17**, respectively; Lane 3 = relaxed plasmid DNA marker; Lane 4 = supercoiled DNA; Lane 5 = supercoiled DNA + Top I; Lanes 6 = supercoiled DNA + Top I + CPT. (b) Lanes 1-2 = supercoiled DNA + Top I + chromones **19** and **18**, respectively; Lane 3 = supercoiled DNA + Top I; Lanes 4 = supercoiled DNA + Top I + CPT; Lane 5 = relaxed plasmid DNA marker; Lane 6 = supercoiled DNA. (c) Lane 1 = relaxed plasmid DNA marker; Lane 2 = supercoiled DNA; Lane 3 = supercoiled DNA + Top I; Lane 4 = supercoiled DNA + Top I + CPT; Lanes 5-7 = supercoiled DNA + Top I + chromones **23**, **22** and **21**, respectively. (d) Lanes 1-4 same as (c); Lanes 5-6 = supercoiled DNA + Top I + chromones **25** and **24**, respectively.

CoMFA study

In order to investigate the structure-Top I inhibitory activity relationship, 3D QSAR CoMFA and CoMSIA were performed. Eighteen chromones (whose % inhibition were determined at 20 μM) were used as data set (Table 3), of which 5 compounds were chosen as test set while the remaining 13 compounds were treated as training set. The selected test set represented a range of activity similar to that of the training set and was used to evaluate the predictive power of the CoMFA and CoMSIA models. The percentage inhibition was converted to log % inhibition and used as dependent variables for 3D QSAR study.

Table 3. Structures and Top I inhibitory activity of chromones in the data set used in CoMFA and CoMSIA studies.

Compd	R_2	R_3	R_5 R_6 R_7	R_8	% inhibition	log % inhibition
Training set						
2	Phenyl	Benzoyl	H H O-[3‴-(OCH_3)-benzoyl]	H	62.63	1.797
3	Phenyl	Benzoyl	H H O-[4‴-(OCH_3)-benzoyl]	H	52.37	1.719
4	Phenyl	Benzoyl	H H O-[3‴-(NO_2)-benzoyl]	H	63.96	1.806
6	3′-(OCH_3)-phenyl	3″-(OCH_3)-benzoyl	H H O-Benzyl	H	44.54	1.649
7	3′-(OCH_3)-phenyl	3″-(OCH_3)-benzoyl	H H O-[3‴-(OCH_3)-benzyl]	H	33.41	1.524
8	3′-(OCH_3)-phenyl	3″-(OCH_3) benzoyl	H H O-Benzoyl	H	48.68	1.687
11	4′-(OCH_3)-phenyl	4″-(OCH_3)-benzoyl	H H O-[3‴-(OCH_3)-benzyl]	H	47.76	1.679
12	4′-(OCH_3)-phenyl	4″-(OCH_3)-benzoyl	H H O-Benzoyl	H	55.77	1.746
13	4′-(OCH_3)-phenyl	4″-(OCH_3)-benzoyl	H H O-[3‴-(OCH_3)-benzoyl]	H	39.78	1.600
14	4′-(OCH_3)-phenyl	4″-(OCH_3)-benzoyl	H H O-[4‴-(OCH_3)-benzoyl]	H	42.66	1.630
15	4′-(NO_2)-phenyl	4″-(NO_2)-benzoyl	H H O-Benzoyl	H	66.03	1.820
16	4′-(NO_2)-phenyl	4″-(NO_2)-benzoyl	H H O-[3‴-(NO_2)-benzoyl]	H	64.73	1.811
20	4′-(NO_2)-phenyl	4″-(NO_2)-benzoyl	H H OH	H	92.00	1.964
Test set						
1	Phenyl	Benzoyl	H H O-Benzyl	H	52.03	1.716
5	Phenyl	Benzoyl	H H O-[4‴-(NO_2)-benzoyl]	H	50.63	1.704
9	3′-(OCH_3)-phenyl	3″-(OCH_3)-benzoyl	H H O-[3‴-(OCH_3)-benzoyl]	H	58.76	1.769
10	3′-(OCH_3)-phenyl	3″-(OCH_3)-benzoyl	H H O-[4‴-(OCH_3)-benzoyl]	H	50.23	1.701
19	4′-(OCH_3)-phenyl	4″-(OCH_3)-benzoyl	H H OH	H	42.06	1.624

Field fit and align database methods were the two alignment criteria used in the 3D QSAR study. The CoMFA model obtained from field fit alignment gave better statistical results than align database alignment (data not shown). Any field column the deviation of which was less than 2.0 kcal/mole in magnitude was excluded as well as any lattice point the energy of which exceeded 30 kcal/mole was ignored from the PLS analysis. The best CoMFA model gave cross-validated r^2 (q^2) = 0.578 and non cross-validated r^2 = 0.995 (Table 4), using traditional CoMFA steric and electrostatic fields. The steric and electrostatic fields contributed to the QSAR equation by 60.8 % and 39.2 0%, respectively, which suggested that variation in the Top I inhibitory activity was predominantly determined by steric property. The experimental % inhibitions, the predicted % inhibitions and the residuals of the predictions are shown in Table 5. The scattered plots of the experimental and predicted activities of the compounds in the training set and test set are shown in Figure 2a.

CoMSIA study

The CoMSIA study was performed using the same PLS protocol and stepwise procedure as in the CoMFA study. The best CoMSIA model gave q^2 = 0.632, r^2 = 0.996 and included electrostatic, steric, and hydrophobic fields. In this CoMSIA model,

steric, electrostatic, and hydrophobic fields contributed to the QSAR equation by 18.1 %, 46.2 %, and 35.7 %, respectively. The experimental and predicted % inhibition and the scattered plots of both training set and test set are shown in Table 5 and Figure 2b, respectively.

Table 4. CoMFA and CoMSIA statistical results.

		CoMFA	CoMSIA
	Number of molecules in training set	13	13
	Number of molecules in test set	5	5
Cross-validation	Optimal components	5	6
	q^2	0.578	0.632
	S	0.098	0.099
Non cross-validation	r^2	0.995	0.996
	S	0.011	0.011
	F	287.013	228.997
Contributions	Steric	0.608	0.181
	Electrostatic	0.392	0.462
	Hydrophobic		0.357

Table 5. Experimental (observed), predicted activities and the residuals of CoMFA and CoMSIA models.

Compd.	log % inhibition				
	CoMFA			CoMSIA	
	Experimental	Predicted	Residual	Predicted	Residual
Training set					
2	1.797	1.806	-0.009	1.795	0.002
3	1.719	1.724	-0.005	1.714	0.005
4	1.806	1.799	0.007	1.809	-0.003
6	1.649	1.630	0.019	1.640	0.009
7	1.524	1.536	-0.012	1.540	-0.016
8	1.687	1.692	-0.005	1.690	-0.003
11	1.679	1.682	-0.003	1.676	0.003
12	1.746	1.744	0.002	1.749	-0.003
13	1.600	1.593	0.007	1.586	0.014
14	1.630	1.632	-0.002	1.638	-0.008
15	1.820	1.819	0.001	1.817	0.003
16	1.811	1.812	-0.001	1.809	0.002
20	1.964	1.963	0.001	1.969	-0.005
Test set					
1	1.716	1.816	-0.100	1.807	-0.091
5	1.704	1.828	-0.124	1.769	-0.065
9	1.769	1.620	0.149	1.604	0.165
10	1.701	1.615	0.086	1.612	0.089
19	1.624	1.955	-0.331	1.791	-0.167

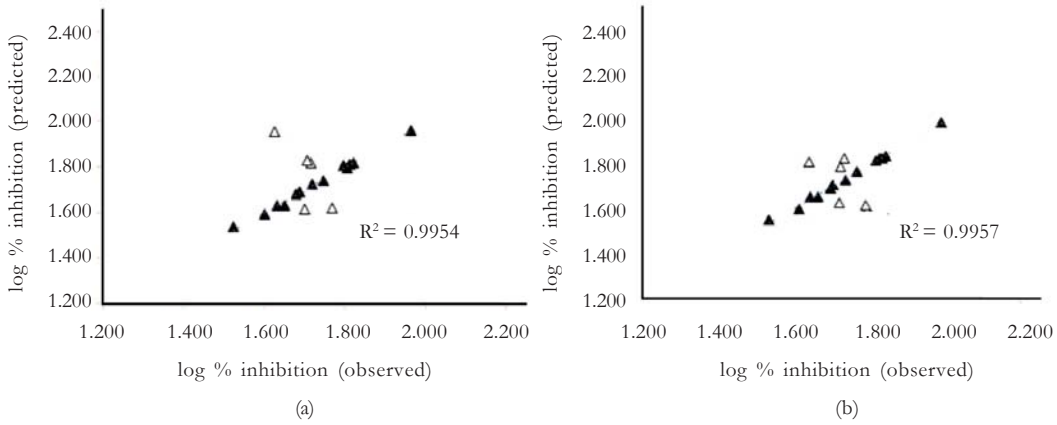

Figure 2. Predicted and observed (experimental) activity for the training set (%) and the test set (Δ). (a) CoMFA model. (b) CoMSIA model.

CoMFA and CoMSIA contour maps

The QSARs produced by CoMFA and CoMSIA models, which are usually represented as 3D "coefficient contour maps" are shown in Figures 3 and 4, respectively. The molecular structure of the most potent chromone **20** and the second most potent chromone **15** were displayed inside the field as the reference structures.

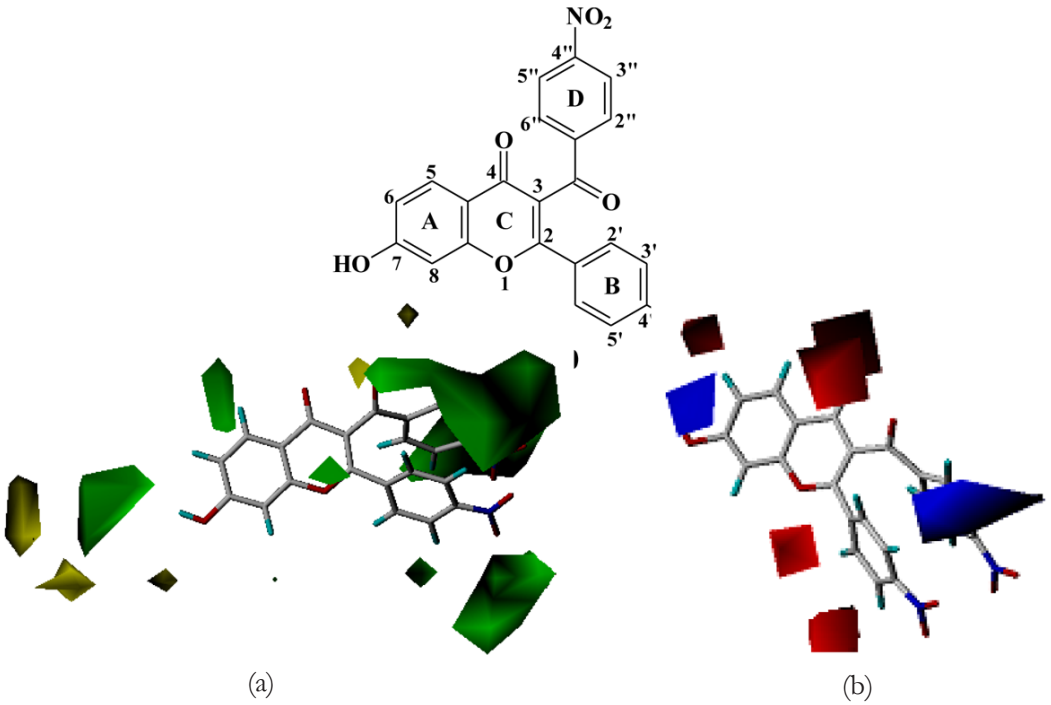

Figure 3. CoMFA contour map. (a) CoMFA steric contour map and (b) electrostatic contour map. The green contours refer to sterically favored region; the yellow contours indicate disfavored areas. The blue contours indicate region where electropositive substituent is favored and red contours refer to region where electronegative substituent is favored.

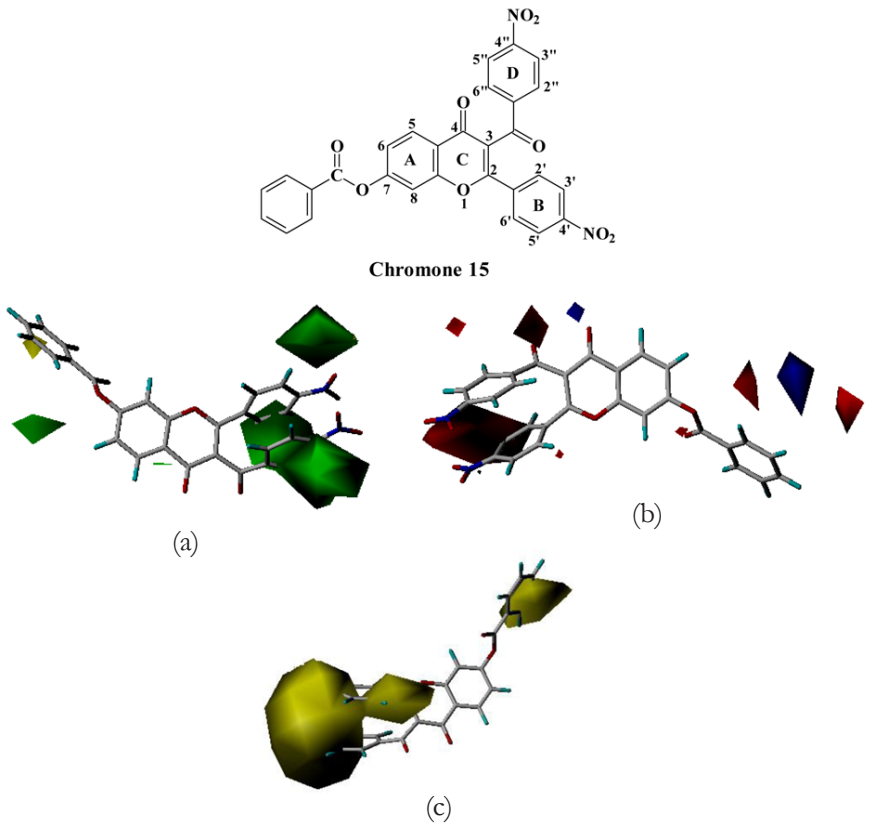

Figure 4. (a) CoMSIA setric contour map. (b) CoMSIA electrostatic contour map. (c) CoMSIA hydrophobic contour map, yellow contours indicate region where hydrophobic group is favored.

The CoMFA and CoMSIA steric contour maps (Figures 3a and 4a, respectively) illustrate common field features. The steric contour maps indicate that bulky substituents should be located around C-4′ of ring B, and C-4″ of ring D. This steric contours (corresponding to the hydrophobic contour map from CoMSIA, Figure 4c) show the yellow regions at C-7, C-4′ and C-4″. These yellow polyhedra indicate that the hydrophobic groups increase the activity. Based on the same substitutions at C-2 and C-3, these results explain the good inhibitory activity of chromones **15**, **16**, and **20** (with exception of chromones **24** and **25** which exhibited only moderate activity). Although the electrostatic contour maps from CoMFA (Figure 3b) and CoMSIA (Figure 4b) are not quite similar, they do show a common field feature that the electropositive substituent (the blue contours) should be located around C-7 of chromone ring and the electronegative group at C-3′ of ring B.

Figures 5a and 5b illustrate the hydrogen bonding interactions between the two most potent compounds, chromones **19** and **20**, and Top I, respectively. The 7-OH group of both chromones formed hydrogen bonding interaction with Asp533 of Top I.

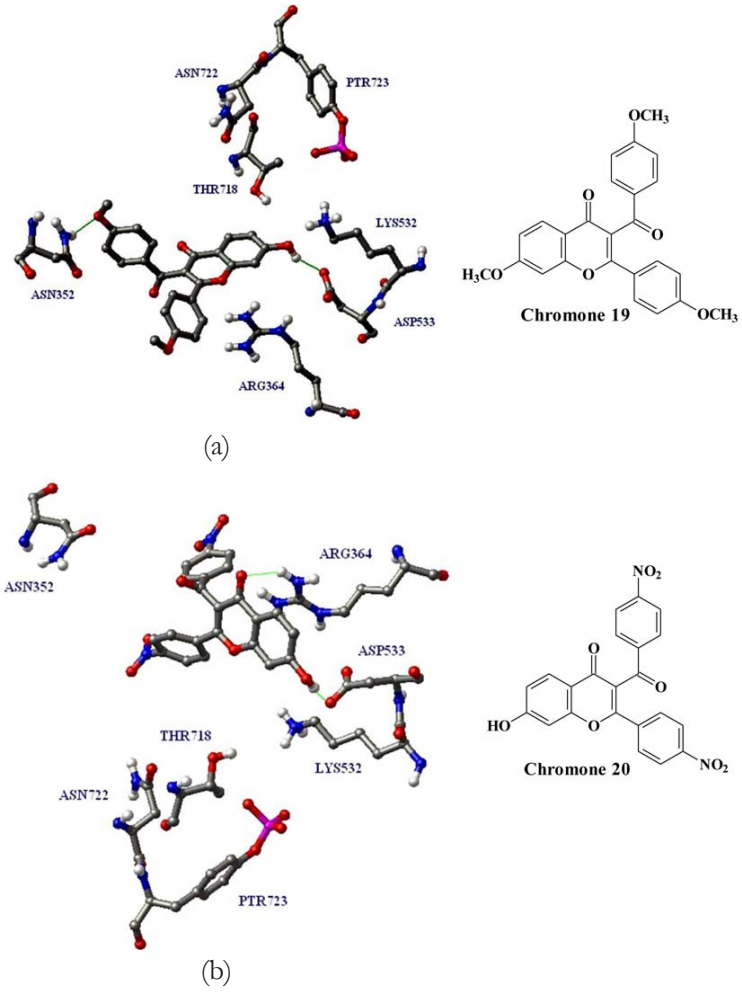

Figure 5. Hydrogen bonding interactions between DNA Top I (1T8I) and (a) chromone **19;** (b) chromone **20**.

4. CONCLUSION

In this study, chromone **20** showed higher inhibitory activity against Top I than the previously reported chromone compounds. The ligand-based 3D QSAR, CoMFA and CoMSIA have been applied to a set of chromone series. Statistical parameters indicate that the established CoMFA and CoMSIA models are reliable. The contour maps provide relationships between structural features and Top I inhibitory activity. They suggest that steric groups at C-4′ (ring B) and C4′′ (ring D), electropositive substituent at C-7 (chromone ring), and electronegative substituent at C-3′ (ring B) are favorable to activity. The 3D QSAR results give the meaningful structural insights into possible modifications of chromone derivatives which could improve activity for the future work.

ACKNOWLEDGEMENT

The authors thank High Performance Computer Center (HPCC), National Electronics and Computer Technology Center (NECTEC) of Thailand for providing SYBYL-X 2.0 facilities.

REFERENCES

[1] Gupta M., Fujimori A. and Pommier Y., *Biochim. Biophys. Acta*, 1995; **1262**: 1-14. DOI 10.1016/0167-4781(95)00029-G.

[2] Wang J.C., *J. Biol. Chem*., 1991; **266**: 6659-6662.

[3] Wang J.C., *Annu. Rev. Biochem*., 1996; **65**: 635-692. DOI 10.1146/annurev.bi.65.070196.003223.

[4] Been M.D. and Champoux J.J., *J. Mol. Biol*., 1984; **180**: 515-532. DOI 10.1016/0022-2836(84)90025-1.

[5] Pommier Y., *Biochimie*, 1998; **80**: 255-270. DOI 10.1016/S0300-9084(98)80008-4.

[6] Champoux J.J., *Annu. Rev. Biochem*., 2001; **70**: 369-413. DOI 10.1146/annurev.biochem.70.1.369.

[7] Champoux J.J., *Prog. Nucleic Acid Res. Mol. Biol*., 1998; **60**: 111-132. DOI 10.1016/S0079-6603(08)60891-0.

[8] Berger J.M., *Biochim. Biophys. Acta*, 1998; **1400**: 3-18. DOI 10.1016/S0167-4781(98)00124-9.

[9] Liu L.F., *Annu. Rev. Biochem*., 1989; **58**: 351-375. DOI 10.1146/annurev.bi.58.070189.002031.

[10] Palumbo M., Gatto B., Moro S., Sissi C. and Zagotto G., *Biochim. Biophys. Acta*., 2002; **1587**: 145-154. DOI 10.1016/S0925-4439(02)00077-7.

[11] Rothenberg M.L., *Ann. Oncol*., 1997; **8**: 837-855. DOI 10.1023/a:1008270717294.

[12] Wall M.E., Wani M.C., Cook C.E., Palmer K.H., McPhail A.I. and Sim G.A., *J. Am. Chem. Soc*., 1966; **88**: 3888-3890. DOI 10.1021/ja00968a057.

[13] Hsiang Y.H., Hertzberg R., Hecht S. and Liu L.F., *J. Biol. Chem*., 1985; **260**: 14873-14878.

[14] Jaxel C., Capranico G., Kerrigan D., Kohn K.W. and Pommier Y., *J. Biol. Chem*., 1991; **266**: 20418-20423.

[15] Staker B.L., Feese M.D., Cushman M., Pommier Y., Zembower D., Stewart L. and Burgin A.B., *J. Med. Chem*., 2005; **48**: 2336-2345. DOI 10.1021/jm049146p.

[16] Marchand C., Antony S., Kohn K.W., Cushman M., Ioanoviciu A., Staker B.L., Burgin A.B., Stewart L. and Pommier Y., *Mol. Cancer Ther*., 2006; **5**: 287-295. DOI 10.1158/1535-7163.MCT-05-0456.

[17] Constantinou A., Mehta R., Runyan C., Rao K., Vaughan A. and Moon R., *J. Nat. Prod*., 1995; **58**: 217-225. DOI 10.1021/np50116a009.

[18] Boege F., Straub T., Kehr A., Boesenberg C., Christiansen K., Andersen A., Jakob F. and Kohrle J., *J. Biol. Chem*., 1996; **271**: 2262-2270. DOI 10.1074/jbc.271.4.2262.

[19] Das B.B., Sen N., Roy A., Dasgupta S.B., Ganguly A., Mohanta B.C., Dinda B. and Majumder H.K., *Nucleic Acids Res*., 2006; **34**: 1121-1132. DOI 10.1093/nar/gkj502.

[20] Chowdhury A.R., Sharma S., Mandal S., Goswami A., Mukhopadhyay S. and Majumder H.K., *Biochem. J*., 2002; **366**: 653-661. DOI 10.1042/bj20020098.

[21] Maicheen C., Jittikoon J., Vajragupta O. and Ungwitayatorn J., *Med. Chem*., 2013; **9**: 329-339. DOI 10.2174/1573406411309030003.

[22] Vladu B., Woynarowski J.M., Manikumar G., Wani M.C., Wall M.E., Von Hoff D.D. and Wadkins R.M., *Mol. Pharmacol*., 2000; **57**: 243-251.

[23] Jaxel C., Kohn K.W., Wani M.C. and Wall M.E., *Cancer Res*., 1989; **49**: 1465-1469.

[24] Hertzberg R.P., Caranfa M.J. and Hecht S.M., *Biochem.*, 1989; **28**: 4629-4638. DOI 10.1021/bi00437a018.

[25] Cramer R.D., Patterson D.E. and Bunce J.D., *J. Am. Chem. Soc.*, 1988; **110**: 5959-5967. DOI 10.1021/ja00226a005.

[26] Klebe G., Abraham U. and Meitzner T., *J. Med. Chem.*, 1994; **37**: 4310-4346. DOI 10.1021/jm00050a010.

[27] Klebe G. and Abraham U., *J. Comput.-Aided Mol. Des.*, 1999; **13**: 1-10. DOI 10.1023/A:1008047919606.

[28] Riva C., De Toma C., Donadel L., Boi C., Pennini R., Motta G. and Leonardi A., *Synthesis*, 1997; **1997(2)**: 195-201. DOI 10.1055/s-1997-1168.

[29] Ungwitayatorn J., Wiwat C., Samee W., Nunthanavanit P. and Phosrithong N., *J. Mol. Struct.*, 2011; **1001**: 152-161. DOI 10.1016/j.molstruc.2011.06.035.

[30] Pavillard V., Agostini C., Richard S., Charasson V., Montaudon D. and Robert J., *Cancer Chemother. Pharmacol.*, 2002; **49**: 329-335. DOI 10.1007/s00280-001-0416-0.